Journal of Atomic and Molecular Sciences

ISSN 2075-1303

Global Science Press

Influences of cell-penetrating peptide concentration on the penetration of phospholipid membrane

Received Oct. 28, 2017,
Accepted Dec. 18, 2017,

DOI: 10.4208/jams.102817.121817a

http://www.global-sci.org/jams/

Qi Wu[a], Kun Wu[a], and Qingtain Meng[a]*

Abstract. It is necessary to fully understand the interaction between the cell penetration peptide and the different types of phospholipid membranes. In this research the interaction between R9 antibacterial peptide and asymmetric phospholipid is studied by using the method of coarse-grained dynamic simulation. The investigation shows that when there is only one R9 antibacterial peptide in the system, it is hard to penetrate through the phospholipid membrane spontaneously. When the concentration of the antibacterial peptide reaches a certain value, with the help of the enhanced electrostatic interactions and the cooperative effect, the peptides will pass through the phospholipid bilayer and reach the inside of the cell. Increasing the concentration of antimicrobial peptides is helpful to improve the penetration rate of the peptides. Our results can provide some theoretical guidance for drug delivery in the biological system.

1. Introduction

Cell-penetrating peptides (CPPs), because of their ability to cross cellular membranes alone or with cargo and deliver bioactive molecules efficiently, have recently gained increasing attention from both the theoretical and experimental researchers [1-3]. As the short sequences of amino acids being usually highly cationic and hydrophilic, they can penetrate membrane more efficiently than others such as trans-activator of transcription (TAT) peptide and polylysine [4]. Since the ability of arginine-rich peptides to facilitate bioactive molecules going into cells makes them promising candidates for drug delivery, it is necessary to investigate the translocation mechanism of polyarginine peptides. During these years, many works related to peptide translocation have been done theoretically or experimentally. For instance, studies have reported that cells can internalize arginine-rich peptides by macropinocytic uptake [5]. Some experimental results indicate that the addition of penetration to brain lipids can induce inverted micelles formation [6]. Although many different classes of CPPs have been studied, the underlying mechanism with which arginine-rich peptides penetrate the cell membranes is still not understood. Thus, the exact pathway through which CPPs enter cells remains incompletely understood.

Apart from the properties of the CPPs, membrane properties may also play an important role in the translocation. Some previous studies have considered the biomembranes as symmetric [7], however most eukaryotic cell membranes are asymmetric. For example, human erythrocyte membrane comprises phosphatidyl- choline, sphingomyelin, and glycolipids in the outer leaflet, and phosphatidylethanolamine, phosphatidylserine, and phosphatidyl- inositol in the inner leaflet [8,9]. Such asymmetry of membrane can affect biological behaviors, such as recognition by macrophages [10] and cellular uptake [11]. Therefore, we think that it is very important to further study the CPPs' translocation across asymmetric lipid bilayer. Because of the higher translocation efficiency than other CPPs, polyarginine peptides (R9) are always the focuses of many investigations. Li et al. [12] have shown that multiple polyarginine peptides can penetrate asymmetric membranes cooperatively and translocate across membranes while carrying conjugated nanoparticles (NPs). To explore the interactions between NPs and biomembranes, the coarse-grained molecular dynamics (CGMD) simulations have recently become a powerful and indispensable tool [13-15]. In the present study, we will use the CGMD simulations to investigate the effects of R9 peptide concentrations and membrane asymmetric level on the translocation mechanism. Our study may provide insights into the mechanism of interactions between peptides and asymmetric membranes at molecular level, which can impact targeted gene and drug delivery.

2. Model and Methods

CGMD simulations are used to investigate the interactions between CPPs and biomembrane because they present larger spatial and temporal scales comparing with all-atom molecular dynamics simulations [16,17]. In this paper, we will use the Martini coarse graining (CG) force field [18] to study the translocation process of the polyarginines. This force field defines four particle types, i.e., polar(P), nonpolar(N), apolar(C), and charged (Q). Within a main type, subtypes are either distinguished by one or two letters denoting the hydrogen-bonding capabilities, i.e., d(donor), a (acceptor), da(both), o(none), or by a number indicating the degree of polarity (from 1, low polarity, to 5, high polarity). It should be stated that because of the smoothed energy barrier in the Martini CG force field, the effective time that the system has experienced is 4 times longer than the simulation sampling time [4], thus in this work the effective time is used to perform the simulation.

School of Physics and Electronics, Shandong Normal University, Jinan, 250014, China
**Corresponding author. E-mail address: qtmeng@sdnu.edu.cn*

To investigate the mechanism of peptides and membrane interactions, it is necessary to have information about the atomistic structure of peptides used. Firstly, the atomistic R9 is downloaded from the site: http://crdd.osdd.net/raghava/cppsite/ [19]. Then, the atomistic structure is converted into the coarse grained mode by using the script martinize.py downloaded from http://md.chem.rug.nl/index.php/tools2/proteins-and-bilayer following the extended Martini force field for proteins (Martini_v2.2) [20]. The CG structure is simulated 100 ns in aqueous solution. Each arginine includes three beads: the backbone bead (P5) and side chain beads (No and Qd) (Figure 2.1). Since the Qd bead bears one positive charge, the whole R9 carries a charge of +9. The bonded interaction parameters for polyarginine peptides are those as bond, angle and dihedral potential energy functions, while nonbonded interactions are represented by the L-J potential and Coulombic energy functions. Takechi et al. [21] have shown that the random coil structure of the short-chain polyarginines remain unchanged when 69 arginines interact with an anionic phospholipid large unilamellar vesicle. We do not consider the change of its helix property during the simulations, because R9 is also a short-chain peptide.

To explore the interactions of membrane and peptides in real human body, in this study an asymmetric human erythrocyte membrane model [8] is used, which includes three lipid types: dipalmitoyl phosphatidylcholine (DPPC), dipalmitoyl phosphatidy-lethanolamine (DPPE), and dipalmitoyl phosphatidylserine (DPPS). Mapping of lipid molecules based on the Martini CG force field (Martini_v2.2) [22] is shown in Figure 2.2. The lipid choline groups are coarse-grained to the beads Qo, Qd and P5 for DPPC, DPPE and DPPS, respectively. The phosphate groups, glycerol groups and carbon tails of all lipids are represented by Qa, Na and C1, respectively. The expressions and parameters of bonded interactions and nonbonded interactions for lipid in the Martini CG force field are shown in Table 2-1. In the outer leaflet of the membrane, the lipid ratio is 9:1 for DPPC and DPPE, while in the inner membrane leaflet, the lipid ratio is 3:5:2 for DPPC, DPPE, and DPPS, which is similar to the human erythrocyte membrane.

Table 2-1. Detailed description of the lipid model in the Martini CG force field.

Interaction	Type	Equation	Parameter
Nonbonded interaction	L-J potential	$U_{LJ}(r)=4\varepsilon_{ij}\left[(\frac{\sigma_{ij}}{r})^{12}-(\frac{\sigma_{ij}}{r})^{6}\right]$	$\sigma_{ij}=0.47nm$
	Coulombic energy	$U_{el}(r)=\frac{q_i q_j}{4\pi\varepsilon_0\varepsilon_r r}$	$\varepsilon_r=15$
Bonded interaction	Bond potential energy	$V_b=\frac{1}{2}K_b(d_{ij}-d_b)^2$	$K_{bond}=1250\ \mathrm{KJ\ mol^{-1}nm^{-2}}$ $K_{bond}=0.47nm$
	Angle potential energy	$V_a=\frac{1}{2}K_a\left[\cos(\theta_{ijk})-\cos(\theta_a)\right]^2$	K_{angle}=25 $\mathrm{KJ\ mol^{-1}rad^{-2}}$ $\theta_0=180^o$
	Dihedral angle energy	$V_d=K_d\left[1+\cos(n\varphi_{ijkl}-\varphi_d)\right]$	

Figure 2.1: Mapping of R9 peptide in the framework of the Martini force field.

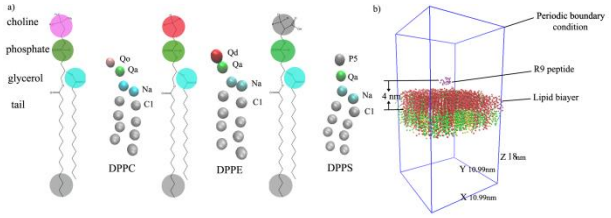

Figure 2.2: a) Mapping of lipid molecules in the framework of the Martini force field. **b)** Detailed information of the simulation box (red, green and yellow represent DPPC DPPE DPPS, respectively.)

Table 2-2. Simulation system

System	Membrane charge	Peptides charge	Ions	Interaction mechanism (penetration amount)
N1	51-	9+	42Na+	Adsorption
N3	51-	27+	24Na+	Adsorption
N5	51-	45+	6Na+	Penetration(1)
N7	51-	63+	12Cl-	Penetration(2)

A cuboid simulation box (only for membrane) with dimensions of 12.5 × 12.5 × 18 nm^3 is created by using the tool insane.py for each simulation system [23] which consists of 510 lipid molecules and approximately 11000 water beads, including 1000 of "antifreeze" (WF) particles to prevent spurious freezing of the Martini solvent at low temperature. The lipid number is similar to the previous studies which are 512 [24]. Sodium ions are added to maintain the neutrality of the systems, the details of which are shown in Table 2-2. Then, the 200 ns NPT equilibration is carried out to relax the system, [11] and the time step is set to 20 fs. The temperature is controlled to 323 K via the V-rescale thermostat with a relaxation time of 0.1 ps. A pressure of 1 bar is maintained with Parrinello-Rahman thermostat and the time constant is 12 ps. A cutoff distance of 1.2 nm is used for van der Waals (vdW) interactions. For electrostatic interactions, the Particle Mesh Ewald (PME) method is employed [25]. The dielectric constant is set to 15 to compensate for the neglect of explicit polarization of the Martini water model [4]. After that, we use the membrane simulated above and rebuild the system by adding the R9 peptides. Detailed information of the system box is provided in Figure 2.2. In the initial state, the center of mass distance in the z-direction between R9 and the membrane (z-distance) is 4 nm. The height of the simulation box is fixed as 18 nm in the z-direction. The systems are first minimized by using the steepest-descent method. Then, a 200 ns NPT equilibration with a force constant 1000 KJ mol^{-1} nm^{-2}

constraint on the peptides and lipid bilayer is conducted to equilibrate water and ions. Finally, the constraint is removed, and a 1000 ns MD simulation for each case in the NPT ensemble is run. The simulations are also carried out at a time step of 20 fs, and the refresh rate of neighbor list is 10 ps. Berendsen thermostat and pressure coupling are used to maintain constant system temperature (323 K) and pressure (1 bar) [26]. The Lennard-Jones (L-J) interaction is cut at 1.2 nm. To reduce the cutoff noise, the L-J potential is smoothly shifted to zero between 0.9 nm and 1.2 nm. The Coulomb interaction is shifted to zero between 0 nm and 1.2 nm also by using the PME method. All simulations are performed by GROMACS 4.6.7 package [27], and results are represented by Visual Molecular Dynamics (VMD) 1.9.2 software [28]. Each simulation is performed at least three times to guarantee the reproducibility of the results.

3. Results and discussion

Here we take R9 peptides with different peptide concentration and an asymmetric membrane without tension as example to study the mechanism of R9-biomembrane interactions. The number ratio of peptides to lipids is used to indicate the peptide concentration (one, three, five, or seven R9 peptides to 510 lipids). We find that due to the presence of high-energy barrier, one and three R9 peptides just absorbing at the outer leaflet of the membrane do not penetrate into the inner leaflet at such low concentrations (Figure 3.1). Li et al [12]. have found and illustrated the similar phenomenon when they investigated the potential of mean force (PMF) in the single R9 and asymmetric membranes interactions.

To further understand the observed interactions, we give the radial distribution functions (RDFs) of lipid groups relative to R9 peptides in Figure 3.2. The highest peak is observed in the lipid phosphate groups (red line in Figure 3.2), the second-highest peak is observed in the glycerol groups (green line in Figure 3.2), and the lowest peak is observed in choline groups (black line in Figure 3.2). The RDFs reflect that R9 peptides are not located in the lipid surface; instead they have been adsorbed at the bottom of lipid head groups. Above results can be attributed to the positively charged R9 peptides attracting negatively charged phosphate groups, meanwhile repulsing positively charged choline groups. He et al. [29] have also observed this phenomenon that peptides accumulate in the bottom membrane leaflet.

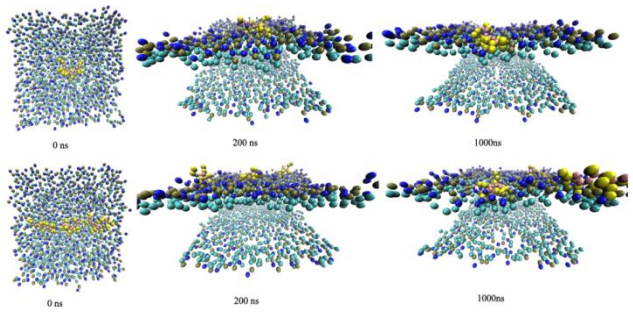

Figure 3.1: The snapshots of interactions between one and three R9 peptides and the asymmetric membrane.

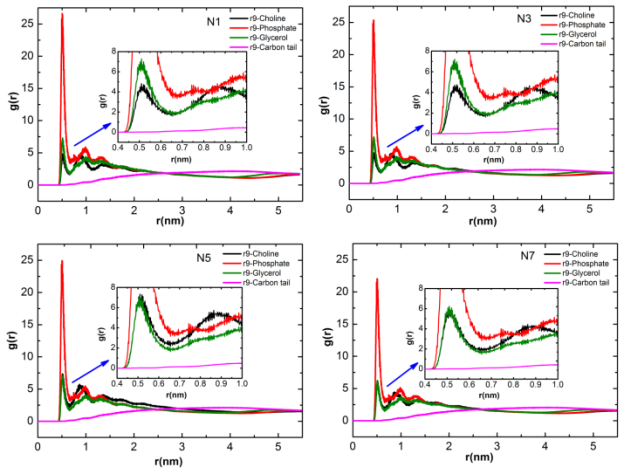

Figure 3.2: RDFs of lipid groups of each system with respect to the R9 peptides.

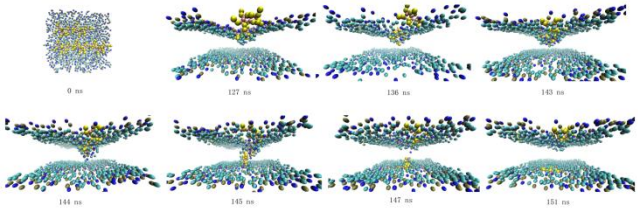

Figure 3.3: Time sequence of snapshots of interactions between five R9 peptides and the asymmetric membrane

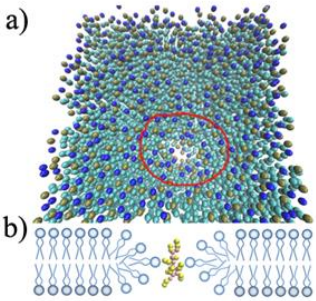

Figure 3.4: a) Top view of the membrane at 144 ns **b)** Schematic of the peptide penetration mechanism

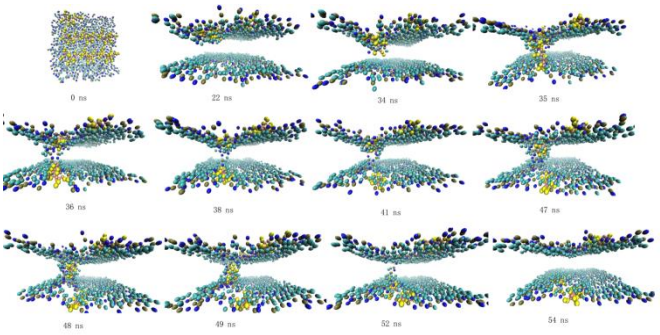

Figure 3.5: Time sequence of snapshots of interactions between seven R9 peptides and the asymmetric membrane

To investigate the case of high R9 concentration, we increase the peptide number as five and seven. Simulation results show that the penetration quantity increases with the number of peptide added into the system (Table 2-2). Here, we show the snapshots of fives peptides interacting with membrane in Figure 3.3. One R9 peptide induces the down ward curvature of the membrane at 127 ns, followed by interacting with the upper leaflet of the membrane. Then, the membrane forms a hole at 144 ns and the R9 peptide penetrates the lipid bilayer along this channel. After 147 ns the peptide thoroughly penetrates the membrane, arrives at the bottom leaflet at around 151 ns, and then the hole disappears. Here we give the top view of membrane hole at 144 ns (Figure 3.4) and penetration mechanism of peptides (Figure 3.4), and for clarity the peptides are not shown in the Figure 3.4. From the top and side view of the membrane, we can infer that the hole is hydrophilic, i.e., water molecules do not penetrate membrane along it. The snapshots of seven peptides interacting with membrane are shown in Figure 3.5. Because of the increased concentration of peptides, one peptide can induce quickly the downward curvature of membrane at 22 ns. Then the peptide begins to penetrate into the membrane following the pattern above. After 38 ns the first peptide thoroughly penetrates the membrane and the second peptide begins to interact with membrane at 41 ns. It is found that the hole has always existed during this time. After 54 ns the second peptide also penetrates the membrane and then the hole disappears. This result is similar to a previous experimental study which reported that the random coil structure of arginine-rich CPPs does not induce permanent membrane damage after penetration [30]. The z-distance between the mass center of peptides and bilayer can further indicate that how many peptides penetrate into the inner membrane leaflet (Figure 3.6).

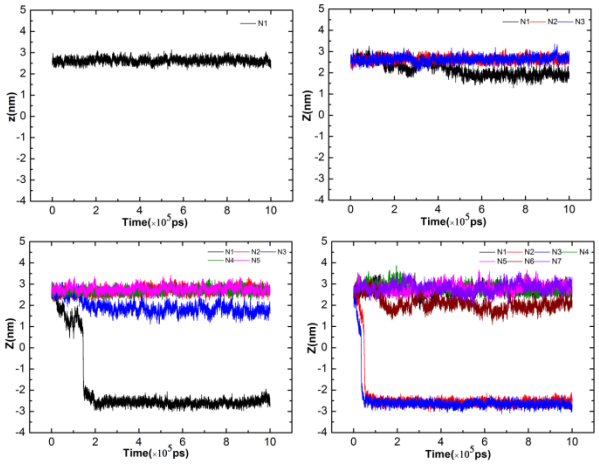

Figure 3.6: Time sequence of the center of mass distance in the z direction (z-distance) between peptides and the membrane

There are two reasons to explain this phenomenon observed under high R9 concentration. The first involves enhanced electrostatic interactions in the system. Because of the higher concentrations of R9 peptides, more positive charges exist in the system and therefore enhance the electrostatic attraction between peptides and DPPS lipids in the bottom membrane leaflet. Tian et al. [8] have shown that electrostatic interactions are important for the interactions between negatively charged biomembrane and cationic nanoparticles. The other reason is the cooperation effect of peptides. Lee et al. [31] have shown the cooperation effect of polyamidoamine (PAMAM) dendrimers during inserting into a bilayer. Multi-dendrimers induce the forming of the membrane curves and then are located in curved regions to penetrate the membrane. The cooperation effect of multi-R9 peptides also follows this process. The details of penetration process are shown in Figures 3.3 and 3.5. These results indicate that both the high concentration (five and seven peptides to 510 lipids) and the enhanced electrostatic interactions can suppress the energy barrier, which makes it easy for R9 peptides to cross the lipid bilayer.

4. Conclusions

In our study, the method of CGMD simulation is used to investigate the mechanism of the interaction between R9 antimicrobial peptides and asymmetric phospholipid membrane which is very similar to human cell membrane. The simulation results show that because of the presence of the big energy barrier, one peptide can't overcome it and translocate across the phospholipid membrane spontaneously. In contrast, because of the enhanced electrostatic interactions and cooperation effect of multiple peptides, the R9 peptides can cross over the large energy barrier and induce to form a hole in the asymmetric membrane. Then, the peptides translocate across the membrane cooperatively along the channel. The process diagram of peptide through membrane shows that the hole through which peptides pass the membrane is a hydrophilic ring hole, and the water molecules do not pass through the membrane along the channel. As the concentration of antimicrobial peptides increases, the number of the peptides passing through the asymmetric phospholipid membrane has also increased accordingly, the penetration time is also ahead. Our results illustrate the interaction between the antibacterial peptide and the phospholipid membrane at the molecular level and are helpful for drug delivery.

Acknowledgements

This work was supported by National Natural Science Foundation of China (Grant No. 11674198), Taishan scholar project of Shandong Province, and Shandong Province Natural Science Foundation (Grant No. ZR2014AM002).

References

[1] D. M. Copolovici, K. Langel, E. Eriste and U. Langel, ACS nano, 8 (2014) 1972.
[2] C. Bechara and S. Sagan, FEBS letters, 587 (2013) 1693.

[3] A. Bolhassani, Biochimica et Biophysica Acta (BBA)-Reviews on Cancer, 1816 (2011) 232.
[4] S. Futaki, Adv. Drug Deliv. Rev., 57 (2005) 547.
[5] S. Futaki, I. Nakase, A. Tadokoro, T. Takeuchi and A. T. Jones, Biochem. Soc.Trans., 35 (2007) 784.
[6] J. P. Berlose, O. Convert, D. Derossi, A. Brunissen and G. Chassaing, FEBS J., 24 (1996) 372.
[7] H. M. Ding and Y. Q. Ma, Biomaterials, 33 (2012) 5798.
[8] W. D. Tian and Y. Q. Ma, Soft Matter, 8 (2012) 6378.
[9] A. Verkleij, R. Zwaal, B. Roelofsen, P. Comfurius, D. Kastelijn and L. Van Deenen, Biochim. Biophys. Acta., 323 (1973) 178.
[10] S. K. Sahu, S. N. Gummadi, N. Manoj and G. K. Aradhyam, Arch. Biochem. Biophys., 462 (2007) 103.
[11] X. C. He, Z. G. Qu, F. Xu, M. Lin, J. L. Wang, X. H. Shi and T. J. Lu, Soft Matter, 10 (2014) 139.
[12] Z. L. Li, H. M. Ding and Y. Q. Ma, Soft Matter, 9 (2012) 1281.
[13] H. M. Ding and Y. Q. Ma, Small, 11 (2015) 1055.
[14] H. M. Ding, W. D. Tian and Y. Q. Ma, Acs Nano, 6 (2012) 1230.
[15] K. Yang and Y. Q. Ma, Nat. Nanotechnol., 5 (2010) 579.
[16] X. Shi, Y. Kong and H. Gao, Acta Mech. Sinica, 24 (2008) 161.
[17] J. Wang, Y. Wei, X. Shi and H. Gao, Rsc Adv., 3 (2013) 15776.
[18] S. J. Marrink, H. J. Risselada, S. Yefimov, D. P. Tieleman and A. H. De Vries, J. Phys. Chem. B, 111 (2007) 7812.
[19] P. Agrawal, S. Bhalla, S. S. Usmani, S. Singh, K. Chaudhary, G. P. Raghava and A. Gautam, Nucleic Acids Res., 44 (2016) D1098.
[20] L. Monticelli, S. K. Kandasamy, X. Periole, R. G. Larson, D. P. Tieleman and S. J. Marrink, J. Chem. Theory Comput., 4 (2008) 819.
[21] Y. Takechi, H. Yoshii, M. Tanaka, T. Kawakami, S. Aimoto and H. Saito, Langmuir, 27 (2011) 7099.
[22] S. J. Marrink , A. H. De Vries and A. E. Mark, J. Phys. Chem. B, 108 (2004) 750.
[23] T. A. Wassenaar, H. I. Ingólfsson, R. A. Böckmann, D. P. Tieleman and S. J. Marrink, J. chem. Theory Comput., 11 (2015) 2144.
[24] H. Lee and R. G. Larson, J. Phys. Chem. B, 110 (2006) 18204.
[25] U. Essmann, L. Perera, M. L. Berkowitz, T. Darden, H. Lee and L. G. Pedersen, J. Chem. Phys., 103 (1995) 8577.
[26] Y. Li, X. Chen and N. Gu, J. Phys. Chem. B, 112 (2008) 16647.
[27] Van Der Spoel D., E. Lindahl, B. Hess, G. Groenhof, A. E. Mark and H. J. Berendsen, J. Comput. Chem., 26 (2005) 1701.
[28] W. Humphrey, A. Dalke and K. Schulten, J. Mol. Graph., 14 (1996) 33.
[29] X. He, M. Lin, B. Sha, S. Feng, X. Shi, Z. Qu, and F. Xu, Sci. Rep., 5 (2015).
[30] Y. Su, A. J. Waring, P. Ruchala and M. Hong, Biochemistry, 49 (2010) 6009.
[31] H. Lee and R. G. Larson, J. Phys. Chem. B, 112 (2008) 7778.